ACS OMEGA

http://pubs.acs.org/journal/acsodf

Article

Discovery of Hybrid Thiouracil–Coumarin Conjugates as Potential Novel Anti-SARS-CoV-2 Agents Targeting the Virus's Polymerase "RdRp" as a Confirmed Interacting Biomolecule

Published as part of the ACS Omega virtual special issue "Phytochemistry".

Divakar Vishwanath, Anita Shete-Aich, Manjunath B. Honnegowda, Mahesh Padukudru Anand, Saravana Babu Chidambaram, Gajanan Sapkal, Basappa Basappa,* and Pragya D. Yadav*

Cite This: *ACS Omega* 2023, 8, 27056–27066

Read Online

ACCESS | Metrics & More | Article Recommendations | Supporting Information

ABSTRACT: The coronavirus (COVID-19) pandemic, along with its various strains, has emerged as a global health crisis that has severely affected humankind and posed a great challenge to the public health system of affected countries. The replication of severe acute respiratory syndrome coronavirus 2 (SARS-CoV-2) mainly depends on RNA-dependent RNA polymerase (RdRp), a key enzyme that is involved in RNA synthesis. In this regard, we designed, synthesized, and characterized hybrid thiouracil and coumarin conjugates (HTCAs) by ether linkage, which were found to have anti-SARS-CoV-2 properties. Our *in vitro* real-time quantitative reverse transcription PCR (RT-qPCR) results confirmed that compounds such as **5d**, **5e**, **5f**, and **5i** inhibited the replication of SARS-CoV-2 with EC_{50} values of 14.3 ± 0.14, 6.59 ± 0.28, 86.3 ± 1.45, and 124 ± 2.38 μM, respectively. Also, compound **5d** displayed significant antiviral activity against human coronavirus 229E (HCoV-229E). In addition, some of the HTCAs reduced the replication of SARS-CoV-2 variants such as D614G and B.617.2. In parallel, HTCAs in uninfected Vero CCL-81 cells indicated that no cytotoxicity was noticed. Furthermore, we compared the *in silico* interaction of lead compounds **5d** and **5e** toward the cocrystal structure of Suramin and RdRp polymerase with Remdesvir triphosphate, which showed that compounds **5d**, **5e**, and Remdesvir triphosphate (RTP) share a common catalytical site of RdRp but not Suramin. Additionally, the *in silico* ADMET properties predicted for the lead HTCAs and RTP showed that the maximum therapeutic doses recommended for compounds **5d** and **5e** were comparable to those of RTP. Concurrently, the pharmacokinetics of **5d** was characterized in male Wistar Albino rats by administering a single oral gavage at a dose of 10 mg/kg, which gave a Cmax value of 0.22 μg/mL and a terminal elimination half-life period of 73.30 h. In conclusion, we established a new chemical entity that acts as a SARS-CoV-2 viral inhibitor with minimal or no toxicity to host cells in the rodent model, encouraging us to proceed with preclinical studies.

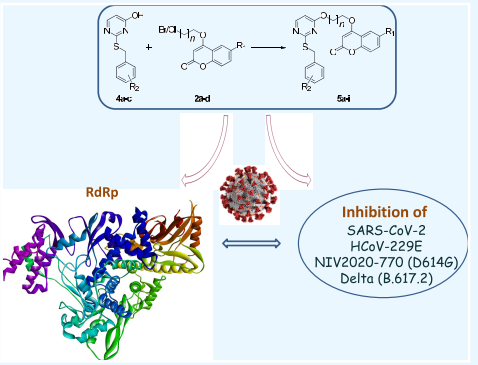

INTRODUCTION

Coronavirus (COVID-19)[1] is a positive, single-stranded RNA that induces severe respiratory infections (SARS-CoV-2), which emerged in late 2019 from Wuhan, China.[2,3] As a result of its widespread occurrence and rapid human transmission leading to loss of lives, the World Health Organization (WHO) officially declared it a pandemic.[4−6] As of April 6, 2023, human SARS-CoV-2 viral transmission has reached 762,201,169 cases and 6,893,190 confirmed deaths across the globe.[7] Additionally, the mutated RNA of SARS-CoV-2 has given rise to resistant and virulent novel variants, imposing a significant burden on the scientific community to develop successful medicines and vaccines.[8−10] Although existing vaccines and drugs can reduce the severity of the disease, there is some cause for concern about the efficacy of vaccines in the context of increasing numbers of mutations.[11−14] Despite many possible targets, the RdRp (nsp12) complex is responsible for RNA replication and represents an ideal target for innovative RdRp inhibitors.[15−17] The use of RdRp has been a crucial strategy for treating several viral infections, including hepatitis C (HCV),[18,19] dengue,[20,21] zika,[20,22] influenza,[23,24] etc. Based on structural disparities and the mode of action, RdRp inhibitors can be categorized into two groups: nucleoside/nucleotide analogues (NAs) and

Received: March 28, 2023
Accepted: June 15, 2023
Published: July 14, 2023

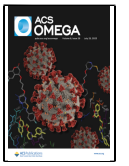

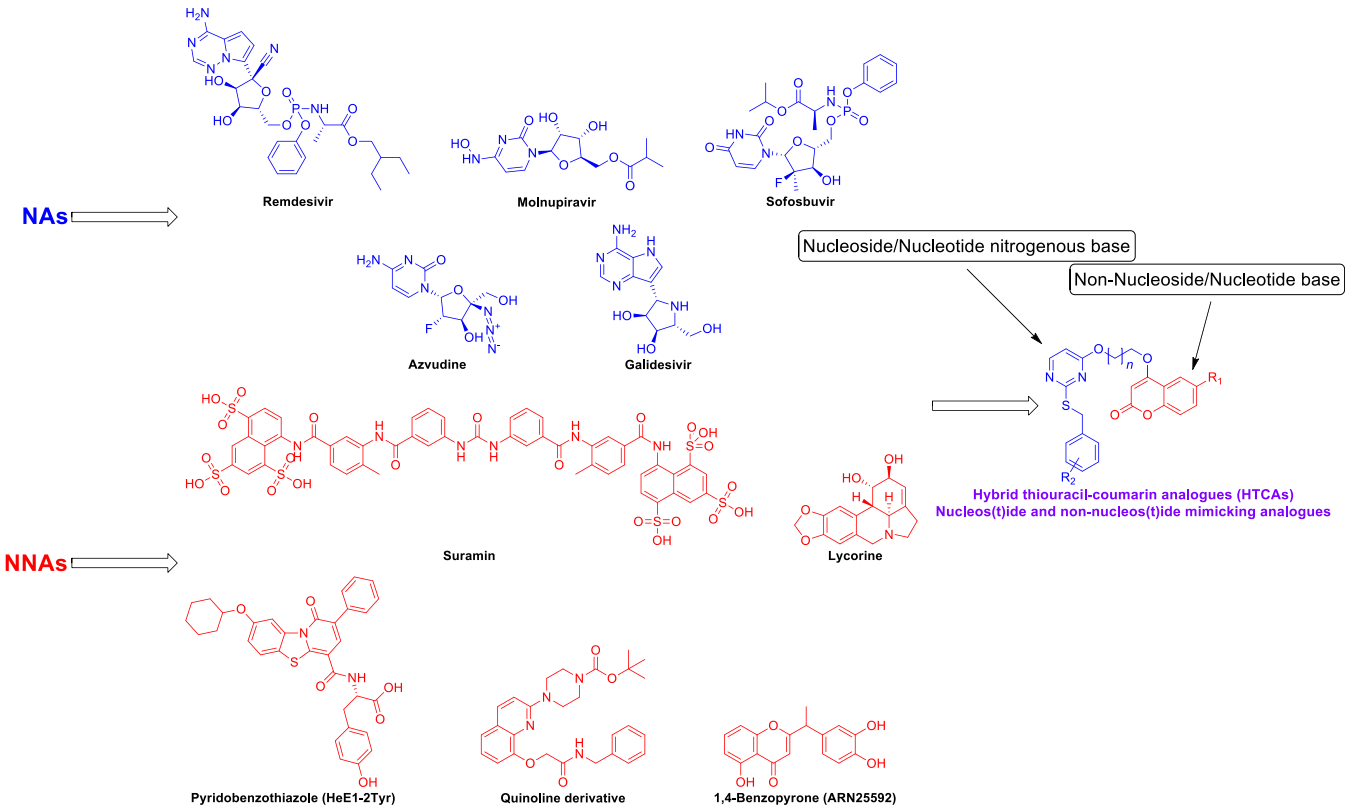

Figure 1. HTCA scaffold evolution that targets RdRp of the SARS-CoV-2 virus.

Scheme 1. Schematic Diagram Showing the Synthesis of Designed HTCAs[a]

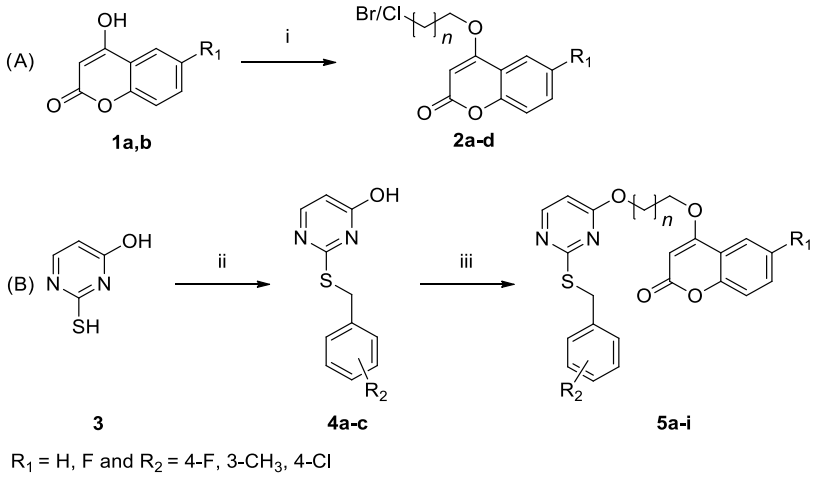

[a](A) Coumarin-Based Alkyl Halide's Synthetic Scheme; (B) Title Compound's Synthetic Scheme. **Reagents and conditions:** (i) 1,2-dibromoethane/1-bromo-3-chloropropane, DMF, K_2CO_3, reflux; (ii) substituted benzyl bromides/benzyl chlorides, EtOH: H_2O (1:1), KOH, 45 °C; (iii) **2a−d**, acetone, K_2CO_3, reflux.

non-nucleoside/nucleotide analogues (NNAs).[15,25] These nucleoside analogues are transformed into active nucleoside triphosphates by cellular enzymes, which deceive and trick SARS-CoV-2 RdRp and then are incorporated into the strand to stop viral replication.[9,14,25] Some commonly used clinically approved repurposed SARS-CoV-2 nucleoside RdRp inhibitors used to decrease morbidity and mortality are Remdesivir and Molnupiravir.[16,26−29] Other nucleoside RdRp inhibitors include Favipiravir, Galidesivir, Ribavirin, Sofosbuvir, Azvudine, and Taroxaz-26.[8,15,30−34] Meanwhile, non-nucleoside analogues (NNAs) disrupt viral replication by directly binding to the active site of RdRp, which is one of their benefits over NAs.[15,25] To date, only a few RdRp NNAs have been reported.[15] Suramin, which is a NNA that inhibits SARS-CoV-2 RdRp, was tested in antiviral assays, and its mode of action was corroborated by a cryo-EM structure.[35,36] In addition, Lycorine, reported as a NNA, directly inhibits the activity of SARS-CoV-2 RdRp.[37]

Recent studies have identified pyridobenzothiazole (HeE1-2Tyr), 3-thioacetamide indole, quinoline, and 1,4-benzopyrone (ARN25592) as non-nucleoside derivatives that are potent RdRp inhibitors of SARS-CoV-2.[15,35,38,39] Since many NAs

https://doi.org/10.1021/acsomega.3c02079
ACS Omega 2023, 8, 27056−27066

and NNAs are reported as RdRp inhibitors, none are beneficial for prolonged broad-spectrum effectiveness, and a specific CoV-2 drug is still required to inhibit the SARS-CoV-2 variants.[9,15,40] In contrast, we attempted to synthesize a hybrid molecule containing nucleos(t)ide and non-nucleos(t)ide mimicking analogues.

Hence, newer hybrid thiouracil−coumarin analogues (HTCAs) are being developed as potent inhibitors of the SARS-CoV-2 virus and its variants (Figure 1). Moreover, computational studies suggest that the interaction of HTCAs with the RdRp catalytical domain was comparable to RTP.

RESULTS AND DISCUSSION

Chemistry of HTCAs. Initially, compounds **2a−d** were synthesized by reacting 4-hydroxy coumarin/fluoro-substituted coumarin with dihalo alkanes. Thiouracil was derivatized with different benzyl halides, giving compounds **4a−c**. Finally, the coupling of compounds **2a−d** and **4a−c** was carried out using potassium carbonate in acetone media (Scheme 1, Table 1). The obtained HTCAs were characterized by using high-end LCMS, ^{1}H NMR, and ^{13}C NMR techniques as well as melting point.

Table 1. Structural and Physical Data of HTCAs

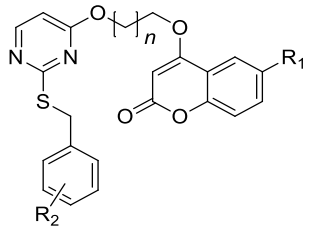

compound code	R_1	R_2	n
5a (PC-01)	H	4-F	1
5b (PC-02)	H	4-F	2
5c (PC-03)	F	4-F	1
5d (PC-04)	F	4-F	2
5e (PC-05)	H	3-CH_3	1
5f (PC-06)	H	3-CH_3	2
5g (PC-07)	F	3-CH_3	1
5h (PC-08)	F	3-CH_3	2
5i (PC-09)	H	4-Cl	1

Anti-SARS-CoV-2 Effects of Hybrid Thiouracil−Coumarin Analogues (HTCAs). Initially, we evaluated the possibility of using HTCAs as SARS-CoV-2 viral inhibitors using the Vero cell line (ATCC, CCL-81) as the host cell.[41] For this purpose, Vero CCL-81 cells (2×10^4 cells/well) were infected with the SARS-CoV-2 virus at a multiplicity of infection (MOI) of 0.01 (200 PFU/well) and incubated for 2 h at 37 °C. Later, the viral input was washed with DMEM, and then, the cells were treated with a medium containing the HTCAs at various concentrations (1.5, 3.75, 7.5, 15, 25, and 50 μM) for 48 h. RT-qPCR of the supernatant of HTCAs and untreated infected cells was performed. The data revealed that the RNA levels decreased upon HTCA treatment in a dose-dependent manner. The most active compounds from HTCAs were found to be **5d**, **5e**, **5f**, and **5i**, whose half-maximal effective concentration (EC_{50}) values were 14.3 ± 0.14, 6.59 ± 0.28, 86.3 ± 1.45, and 124 ± 2.38 μM, respectively. In parallel, the toxicity of HTCAs to Vero cells (1.5, 3.75, 7.5, 15, 25, and 50 μM) was evaluated by treating the Vero CCL-81 cells. We observed that there was no toxicity against tested Vero CCL-81 cells.

Also, inhibition of HTCAs against human coronavirus 229E (HCoV-229E) in the A549 cell line was examined by an MTT colorimetric assay at different concentrations (1.56, 3.13, 6.25, 12.5, and 25 μM), and Oseltamivir was used as a control. Promising antiviral activity was observed for **5d** and **5e** with IC_{50} values of 15.44 and 24.35 μM, respectively. Further, the efficacies of HTCAs were determined on various SARS-CoV-2 variants D614G and B.617.2 at different concentrations (2.5, 10, 25, and 50 μM). Some of the HTCAs were found most effective against both variants with IC_{50} less than 10 μM and have promising selectivity indices (Table 2). All dose−response curves of HTCAs on SARS-CoV-2 and its variants are presented in the Supplementary Figures.

***In Silico* Interactions between HTCAs and RdRp (nsp12) of the SARS-CoV-2 Virus.** Since SARS-CoV-2 had a higher propensity to accept uracil as nucleotide substitution and coumarin-based small molecules were reported to inhibit the RNA polymerases in HCV virus, we hypothesized that HTCAs could target RdRp of the virus.[42] Therefore, the cocrystal structure of Suramin-bound viral RdRp (2.6 Å), determined by cryo-electron microscopy, was utilized (PDB ID: 7d4f).[36] Suramin that bound near the RdRp catalytic site was considered for molecular docking purposes using the

Table 2. Anti-SARS-CoV-2 Effect of HTCAs Using Vero and A549 Host Cells[a,b]

		antiviral effect on SARS-CoV-2 (in the Vero CCL-81 cell line)		antiviral effect on HCoV-229E (in the A549 cell line)		antiviral effect on SARS-CoV-2 NIV2020-770 (D614G variant)		antiviral effect on SARS-CoV-2 Delta (B.617.2 variant)	
compound code	CC_{50} (in μM)	EC_{50} (in μM)	selectivity index	IC_{50} (in μM)	selectivity index	IC_{50} (in μM)	selectivity index	IC_{50} (in μM)	selectivity index
5a (PC-01)	76.80	NS	NA	NS	NA	<50	1.5	<25	3.0
5b (PC-02)	48	NS	NA	NS	NA	<10	4.8	<2.5	19.2
5c (PC-03)	22	NS	NA	NS	NA	<2.5	8.8	<10	2.2
5d (PC-04)	>200	14.3 ± 0.14	13.97	15.44	12.95	<10	20	<10	20
5e (PC-05)	75	6.59 ± 0.28	11.4	24.35	3.06	<25	3	<10	7.5
5f (PC-06)	60	86.3 ± 1.45	<1	NS	NA	<25	2.4	<2.5	24
5g (PC-07)	60	NS	NA	NS	NA	<25	2.4	<10	6
5h (PC-08)	29	NS	NA	NS	NA	<2.5	11.6	<10	2.9
5i (PC-09)	55	124 ± 2.38	<1	NS	NA	<10	5.5	<2.5	22

[a]EC_{50} and IC_{50} of HTCAs against SARS-CoV-2 and SARS-CoV-2 variants are presented, determined by three independent experiments. [b]**Note:** NS, not significant; NA, not applicable.

https://doi.org/10.1021/acsomega.3c02079
ACS Omega 2023, 8, 27056−27066

accelrys DS version 2.5. The sdf file for Suramin, Remdesvir triphosphate (RTP), and the lead SARS-CoV-2 virus inhibitors was prepared for the docking studies.[43,44] Using the reported protocol of the CDOCKER program, we docked the abovementioned ligands to the catalytic site of the RdRP protein structure. The docking scores are summarized. The net CDOCKER interaction energies of RTP, Suramin, **5d**, **5e**, **5f**, and **5i** were found to be −9.09, −19.87, −7.41, −8.43, −7.14, and −3.66 kcal/mole, respectively, indicating that interaction of Suramin with the protein was the best (Figure 2A).

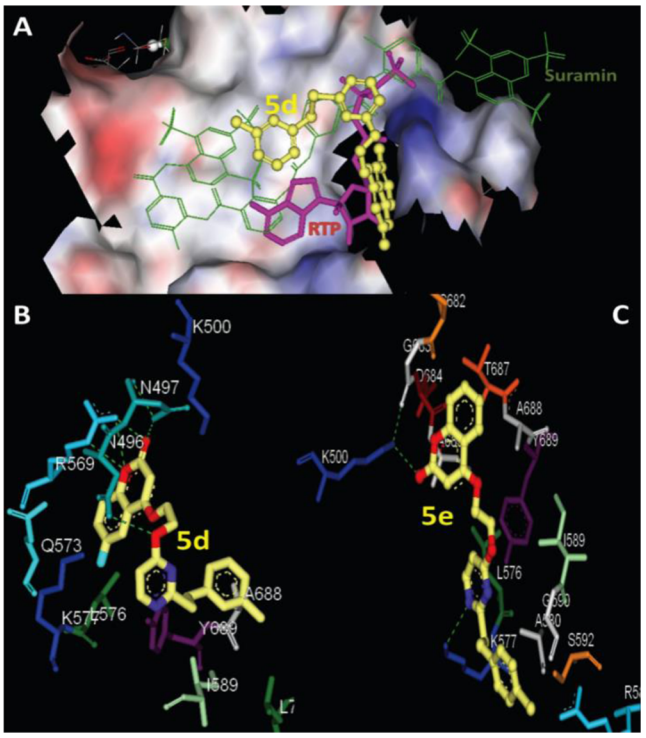

Figure 2. *In silico* molecular interaction studies of HTCAs with the RdRp catalytical domain of the SARS-CoV-2 virus. (**A**) Surface view of the docked compounds such as RTP (pink-colored stick model), Suramin (green-colored line model), and compound **5d** (yellow-colored ball-and-stick model) toward the catalytical domain of RdRp. Interaction maps of key amino acids of RdRp and compounds **5d** (**B**) and **5e** (**C**) are presented with parent amino acid colors.

Molecular docking of compound **5d** at the catalytical site of RdRp of the SARS-CoV-2 virus revealed that the compound **5d** and RTP share a common binding site. The binding mode of the compound **5d** with RdRp can be viewed in three segments, in which the lactone or pyrone ring of **5d** formed *H*-bond interactions with RdRp key amino acid residues N497 and R569. In addition, the fluoro-coumarin ring of compound **5d** formed cation−π stacking and van der Waals interactions with K500, Q573, L576, and K577 residues of the RdRp catalytical domain. Second, the ether linkage of the compound **5d** had hydrogen bonding with N496, indicating the requirement of a linker in the HTCAs. Finally, the benzylated thiouracil was surrounded with the key amino acid residues Y689, A688, I589, and L758, indicating that the interaction of compound **5d** was unique when compared to Suramin. The interaction of compound **5e** with the RdRp catalytical domain was comparable to that of RTP and compound **5d**. However, compound **5e** possessed two inter-hydrogen bondings with the RdRp domain amino acids K500 and K577 by pyrone and uracil rings (Figure 2B,C). Further, *in vitro* interaction studies will explore the structure−activity relationship with respect to the binding of HTCAs to the RdRp protein.

Pharmacological Features of Compound 5d. In order to develop a druglike small molecule that inhibits the SARS-CoV-2 virus, we further tested the lead compound **5d** for acute oral toxicity profile using female rats. The animals were administered a single dose of compound **5d** at 300 and 2000 mg/kg, p.o. and observed for clinical signs of toxicity for 14 days.[45] There were no signs of toxicity and gross pathological changes were observed at 300 mg/kg. However, administration of 2000 mg/kg produced mortality. Based on the above observations, the LD_{50} cutoff value of compound **5d** was found to be 500−1000 mg/kg and classified as Category-4 based on the Globally Harmonized Classification System (GHS) for Chemical Substances and Mixtures. Further, compound **5d** was assessed for its oral bioavailability by feeding male Wistar Albino rats with a single prefixed dose (10 mg/kg, p.o), after being overnight fasted, and blood samples of the animals were collected at different time points through retro-orbital puncture under mild anesthesia and their respective serum was quantitated using HPLC analysis.[46]

The quantification of the chromatogram and other parameters revealed that compound **5d** showed Cmax and

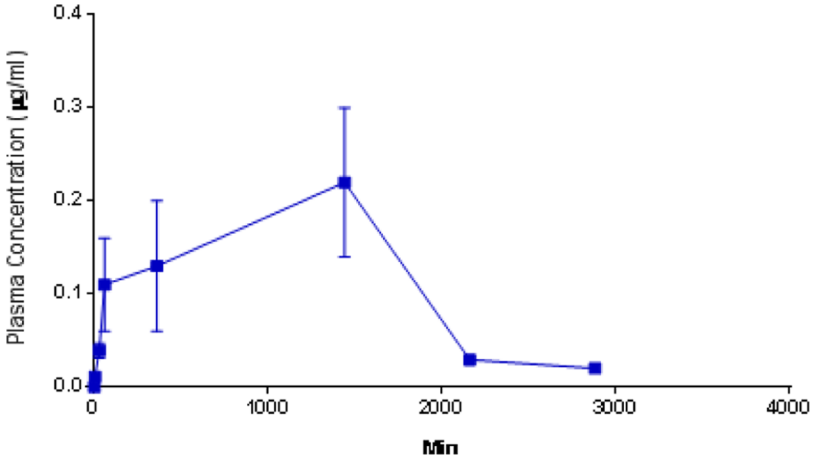

Figure 3. HPLC quantification of compound **5d** in male Wistar Albino rats.

https://doi.org/10.1021/acsomega.3c02079
ACS Omega 2023, 8, 27056−27066

terminal elimination half-life of 0.22 μg/mL and 73.30 h, respectively (Figure 3).

***In Vitro* Metabolic Stability of HTCAs.** Since the liver metabolic stability of HTCAs determines its druglike properties, when we require a longer bioavailability of tested samples. Selective compounds with significant anti-SARS-Cov-2 activities were further subjected to *in vitro* metabolic stability studies. Thus, the liver metabolic stabilities of compounds **5f**, **5h**, **5d**, and **5e** were evaluated by determining the metabolic rates of mouse, rat, and human liver microsomes (Figure 4).[47]

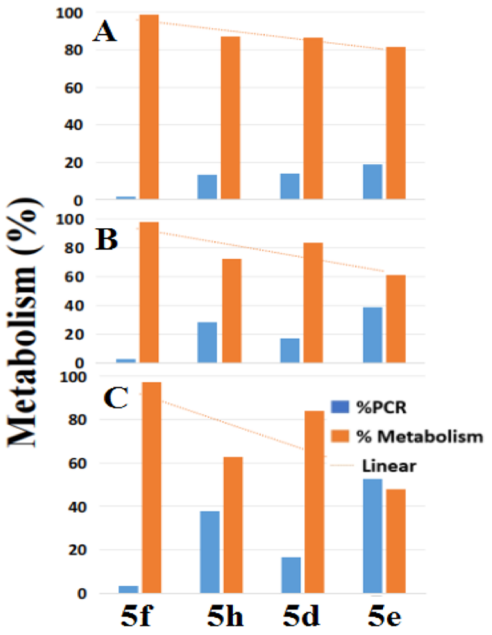

Figure 4. Stability (%) studies of *in vitro* mouse (**A**), rat (**B**), and human (**C**) liver microsomes in the presence of selected HTCAs.

We chose the abovementioned four compounds, as compounds **5d** and **5e** showed broad-spectrum antiviral activity when compared to **5f** and **5h**, which are selective against SARS-CoV-2 variants. Reference drugs such as Verapamil and Atenolol were used, and it was found that these drugs were active toward liver microsomes, which were within the acceptable in-house limits. Among the tested HTCAs, all are metabolized in all tested species to varied extents. At 0.5 h after incubation, >50% of compound **5e** was found to be stable in the human liver microsomes, which was comparable to Atenolol. Thus, compound **5e** showed metabolic stability against rat and human liver microsomes.

ADMET Predictions of Lead HTCAs and Their Comparison to RTP. We further predicted the ADMET properties of lead compounds and compared them with RTP using the computational online vNN-ADMET platform.[48] Around 15 properties associated with ADMET were predicted for compounds **5d**, **5e**, and RTP by using the general protocol of the vNN-ADMET program.[49] The results of the predicted parameters related to *in silico* ADMET properties of compounds **5d**, **5e**, and RTP obtained from the online vNN-ADMET platform server are tabulated in Table 3. A computational study revealed that compounds **5d** and **5e** will not be hepatotoxic, whereas RTP was found to be hepatotoxic. Compound **5e** will not be metabolized rapidly by human liver microsomes, whereas compounds **5d** and RTP do undergo rapid metabolism. In addition, all of the compounds such as **5d**, **5e**, and RTP will not inhibit the isoforms of CYP450s, the common drug metabolizing enzymes. Compound **5e** may pass through the blood–brain barrier (BBB), but both **5d** and RTP were not predicted to cross the blood–brain barrier, an important consideration since the SARS-CoV-2 virus is observed to have significant neurological involvement. These compounds may be substrates for P-glycoprotein, and both compounds **5e** and RTP are inhibitors of P-glycoprotein, whereas **5d** is not. Compounds **5d**, **5e**, and RTP are not inhibitors of matrix metalloproteinases and most likely will not cause chemical mutagenicity. We also determined the maximum therapeutic doses recommended for the lead compounds and compared them to RTP.

CONCLUSIONS

In conclusion, we designed and synthesized novel hybrid thiouracil–coumarin analogues (HTCAs) as SARS-CoV-2 inhibitors. Results of our *in vitro* RT-qPCR data showed that lead HTCAs such as **5d**, **5e**, **5f**, and **5i** reduced the replication of SARS-CoV-2 with minimal or no toxicity to host cells. In addition, some of the HTCAs exhibit significant antiviral activity against human coronavirus 229E (HCoV-229E) and SARS-CoV-2 variants (D614G and B.617.2). Further, the lead HTCAs were taken for *in silico* interactions with the RdRp catalytical domain of the SARS-CoV-2 virus. The *in silico* molecular interaction studies demonstrated that **5d** and RTP share a common catalytical site of RdRp, but not with Suramin. Our pharmacokinetic single-dose toxicity data from rodents showed that the lead compound **5d** could be used for further studies with a relatively better classification of Category-4 based on GHS for Chemical Substances and Mixtures use on animal models. Additionally, the *in silico* ADMET properties showed that the maximum recommended therapeutic dose (MRTD) of lead HTCAs (**5d** and **5e**) was comparable to that

Table 3. vNN-ADMET Predictions of the Lead SARS-CoV-2 Virus Inhibitors and Their Comparison with RTP[a]

	liver toxicity		metabolism: CYP inhibitors for						membrane transporters					others	
query	DILI	CT	HLM	1A2	3A4	2D6	2C9	2C19	BBB	Pgp In	Pgp Sub	hERG	MMP	AMES	MRTD (mg/day)
5d	Y	N	Y	N	N	N	N	N	N	N	Y	Y	N	N	211
5e	N	N	N	N	N	N	N	N	Y	Y	Y	N	N	N	216
RTP	Y	Y	Y	N	N	N	N	N	N	Y	N	N	N	N	229

[a]**Note:** N, No; Y, Yes; DILI, drug-induced liver injury; CT, cytotoxicity; CYP, cytochrome P450; HLM, human liver microsomes; BBB; blood–brain barrier; Pgp, P-glycoprotein; Sub, substrate; In, inhibition; hERG, human ether-a-go-go-related gene; MMP, matrix metalloproteins; AMES; salmonella/microsome mutagenicity; MRTD, maximum recommended therapeutic dose. Online predictions and interpretations using a restricted/unrestricted applicability domain are represented.

https://doi.org/10.1021/acsomega.3c02079
ACS Omega 2023, 8, 27056–27066

of RTP. In conclusion, our results provided that the new chemical entities (NCEs) can help develop drug candidates to target COVID-19 variants in the future.

Experimental Materials and Methods. All chemicals and solvents were purchased from TCI and Sigma-Aldrich. The completion of the reaction was monitored by precoated silica gel TLC plates. The ^{1}H and ^{13}C NMR were recorded on an Agilent NMR spectrophotometer (400 MHz) in $CDCl_3$ using TMS as an internal standard, and chemical shifts are expressed as ppm.[50−53] The mass of the HTCAs was determined by LCMS using a Waters instrument (Xevo G2-XS QTof) (waters column: Sunfire C18, 4.6 mm × 250 mm).

General Procedure for the Synthesis of HTCAs. Substituted 4-hydroxy coumarin (**1a−b**) (1 mmol) was dissolved in dimethylformamide (DMF, 10 mL), and anhydrous potassium carbonate (0.7 mmol) was added. To the above reaction mixture, 1,2-dibromoethane (1 mmol)/1-bromo-3-chloropropane (1 mmol) was added and refluxed at 70 °C with continuous stirring for 2−3 h. After the completion of the reaction (monitored by TLC), the mixture was diluted with water. The precipitate was filtered and washed with water and then purified through column chromatography to obtain alkylated coumarins (**2a−d**).

2-Thiouracil (1 mmol) (**3**) and KOH (1.4 mmol) were dissolved in ethanol/water in a 1:1 ratio. Then, the above reaction mass was heated to 45 °C, and substituted benzyl bromides (1.24 mmol)/benzyl chlorides (1.24 mmol) were added. The completion of the reaction was monitored by TLC. After completion of the reaction, the solvent was evaporated to dryness using a rotary evaporator. Then, the crude obtained was suspended in 10% aqueous $NaHCO_3$ solution and the precipitate was filtered off. Further, the crude was successively washed with water, ethanol, and diethyl ether. The substituted benzyl-2-thiouracils **4a−c** were obtained as white solids.

Finally, **4a−c** (1 mmol) was coupled with **2a−d** (1 mmol) by means of K_2CO_3 (2 mmol) in refluxing acetone. After reaction completion, the solvent was distilled off using a rotary evaporator, and hybrid thiouracil−coumarin analogues (HTCAs) (PC-01 to PC-09) (**5a−i**) were obtained as solids. The solid was filtered off and purified through column chromatography (hexane/ethyl acetate::70:30).

*4-(2-((2-((4-Fluorobenzyl)thio)pyrimidin-4-yl)oxy) ethoxy)-2H-chromen-2-one (**5a**) (PC-01).* **4a** (100 mg, 0.423 mmol) was coupled with **2a** (114 mg, 0.423 mmol) by means of K_2CO_3 (117 mg, 0.847 mmol) in refluxing acetone. After reaction completion, the crude obtained was purified by column chromatography. Compound **5a** was obtained as a white solid (162 mg, 90% yield). MP: 146−148 °C; ^{1}H NMR (400 MHz, $CDCl_3$): δ 8.28 (d, J = 5.6 Hz, 1H, pyrimidine-H), 7.76 (d, J = 7.6 Hz, 1H, chromene-H), 7.61−7.47 (m, 1H, chromene-H), 7.46−7.32 (m, 2H, -C_6H_4), 7.31 (d, J = 8.4 Hz, 1H, chromene-H), 7.31−7.17 (m, 1H, chromene-H), 6.98 (t, J = 8.4 Hz, 2H, -C_6H_4), 6.47 (d, J = 5.6 Hz, 1H, pyrimidine-H), 5.70 (s, 1H, -chromene-H), 4.81 (s, 2H, -CH_2-O), 4.47−4.33 (m, 4H, -CH_2-O (2H), and -CH_2-benzyl (2H)); ^{13}C NMR (100 MHz, $CDCl_3$): δ 171.0, 168.1, 165.2, 163.2, 162.6, 160.8, 157.7, 153.3, 133.2, 132.5, 130.4, 130.3, 123.9, 123.0, 116.7, 115.4, 115.3, 115.2, 104.2, 90.8 (Ar-C), 67.1, 63.5 (-CH_2-O), 34.5 (-CH_2-benzyl); LCMS (ESI): m/z calcd. for $C_{22}H_{17}FN_2O_4S$: 424.4448; found: 425.1093 $[M + H]^+$.

*4-(3-((2-((4-Fluorobenzyl)thio)pyrimidin-4-yl)oxy) propoxy)-2H-chromen-2-one (**5b**) (PC-02).* **4a** (100 mg, 0.423 mmol) was coupled with **2b** (101 mg, 0.423 mmol) by means of K_2CO_3 (117 mg, 0.847 mmol) in refluxing acetone. After reaction completion, the crude obtained was purified by column chromatography. Compound **5b** was obtained as a white solid (160 mg, 86% yield). MP: 138−140 °C; ^{1}H NMR (400 MHz, $CDCl_3$): δ 8.24 (d, J = 5.6 Hz, 1H, pyrimidine-H), 7.78 (d, J = 7.6 Hz, 1H, chromene-H), 7.54 (t, J = 7.2 Hz, 1H, chromene-H), 7.43−7.30 (m, 2H, -C_6H_4), 7.31 (d, J = 8.4 Hz, 1H, chromene-H), 7.31−7.18 (m, 1H, chromene-H), 7.04−6.90 (m, 2H, -C_6H_4), 6.41 (d, J = 5.2 Hz, 1H, pyrimidine-H), 5.69 (s, 1H, chromene-H), 4.63−4.50 (m, 2H, (-CH_2-O), 4.35 (s, 2H, -CH_2-benzyl), 4.34−4.21 (m, 2H, (-CH_2-O), 2.35 (t, J = 5.6 Hz, 2H, (-CH_2-); ^{13}C NMR (100 MHz, $CDCl_3$): δ 171.0, 168.4, 165.4, 163.2, 162.7, 160.72, 157.4, 153.3, 133.3, 132.4, 130.4, 130.3, 123.9, 122.9, 116.8, 115.6, 115.4, 115.2, 104.1, 90.7 (Ar-C), 65.8, 62.6 (-CH_2-O), 34.5 -CH_2-benzyl), 28.1 (-CH_2-); LCMS (ESI): m/z calcd. for $C_{23}H_{19}FN_2O_4S$: 438.4714; found: 439.1230 $[M + H]^+$.

*6-Fluoro-4-(2-((2-((4-fluorobenzyl)thio)pyrimidin-4-yl)-oxy)ethoxy)-2H-chromen-2-one (**5c**) (PC-03).* **4a** (100 mg, 0.423 mmol) was coupled with **2c** (122 mg, 0.423 mmol) by means of K_2CO_3 (117 mg, 0.847 mmol) in refluxing acetone. After reaction completion, the crude obtained was purified by column chromatography. Compound **5c** was obtained as a white solid (161 mg, 86% yield). MP: 126−128 °C; ^{1}H NMR (400 MHz, $CDCl_3$): δ 8.29 (d, J = 5.6 Hz, 1H, pyrimidine-H), 7.49−7.32 (m, 3H, chromene-H), 7.33−7.21 (m, 2H, -C_6H_4), 6.98 (t, J = 8.4 Hz, 2H, -C_6H_4), 6.47 (d, J = 5.6 Hz, 1H, pyrimidine-H), 5.74 (s, 1H, chromene-H), 4.80 (t, J = 4.4 Hz, 2H, -CH_2-O), 4.42 (t, J = 4.4 Hz, 2H, -CH_2-O), 4.38 (s, 2H, -CH_2-benzyl); ^{13}C NMR (100 MHz, $CDCl_3$): δ 171.1, 168.0, 164.4, 163.2, 162.1, 160.7, 159.8, 157.7, 157.4, 149.4, 133.1, 130.4, 130.3, 120.2, 119.9, 118.4, 118.3, 116.4, 116.3, 115.4, 115.2, 109.0, 108.8, 104.1, 91.5 (Ar-C), 67.3, 63.4 (-CH_2-O), 34.5 (-CH_2-benzyl); LCMS (ESI): m/z calcd. for $C_{22}H_{16}F_2N_2O_4S$: 442.4352; found: 443.0991 $[M + H]^+$.

*6-Fluoro-4-(3-((2-((4-fluorobenzyl)thio)pyrimidin-4-yl)-oxy)propoxy)-2H-chromen-2-one (**5d**) (PC-04).* **4a** (100 mg, 0.423 mmol) was coupled with **2d** (109 mg, 0.423 mmol) by means of K_2CO_3 (117 mg, 0.847 mmol) in refluxing acetone. After reaction completion, the crude obtained was purified by column chromatography. Compound **5d** was obtained as a white solid (170 mg, 88% yield). MP: 142−144 °C; ^{1}H NMR (400 MHz, $CDCl_3$): δ 8.24 (d, J = 5.6 Hz, 1H, pyrimidine-H), 7.50−7.37 (m, 1H, chromene-H), 7.42−7.29 (m, 2H, chromene-H), 7.32−7.20 (m, 2H, -C_6H_4), 7.03−6.89 (m, 2H, -C_6H_4), 6.40 (d, J = 5.6 Hz, 1H, pyrimidine-H), 5.71 (s, 1H, chromene-H), 4.55 (t, J = 6.0 Hz, 2H, (-CH_2-O), 4.34 (s, 2H, -CH_2-benzyl), 4.33−4.20 (m, 2H, -CH_2-O), 2.34 (t, J = 6.0 Hz, 2H, -CH_2-); ^{13}C NMR (100 MHz, $CDCl_3$): δ 171.1, 168.3, 164.5, 163.2, 162.3, 160.7, 159.8, 157.4, 157.3, 149.4, 133.2, 130.4, 130.3, 120.0, 119.8, 118.5, 118.4, 116.5, 116.4, 115.4, 115.2, 108.8, 108.6, 104.0, 91.4 (Ar-C), 66.1, 62.6 (-CH_2-O), 34.5 (-CH_2-benzyl), 28.0 (-CH_2-); LCMS (ESI): m/z calcd. for $C_{23}H_{18}F_2N_2O_4S$: 456.4618; found: 457.1150 $[M + H]^+$.

*4-(2-((2-((3-Methylbenzyl)thio)pyrimidin-4-yl)oxy) ethoxy)-2H-chromen-2-one (**5e**) (PC-05).* **4b** (100 mg, 0.430 mmol) was coupled with **2a** (115 mg, 0.430 mmol) by means of K_2CO_3 (119 mg, 0.861 mmol) in refluxing acetone. After reaction completion, the crude obtained was purified by column chromatography. Compound **5e** was obtained as a white solid (168 mg, 93% yield). MP: 140−142 °C; ^{1}H NMR (400 MHz, $CDCl_3$): δ 8.27 (d, J = 5.2 Hz, 1H, pyrimidine-H),

https://doi.org/10.1021/acsomega.3c02079
ACS Omega 2023, 8, 27056−27066

7.76 (d, J = 7.6 Hz, 1H, chromene-H), 7.53 (t, J = 7.2 Hz, 1H, chromene-H), 7.30 (d, J = 8.0 Hz, 1H, chromene-H), 7.28−7.13 (m, 4H, chromene-H (1H), and -C_6H_4 (3H)), 7.06 (d, J = 6.0 Hz, 1H, -C_6H_4), 6.45 (d, J = 5.2 Hz, 1H, pyrimidine-H), 5.66 (s, 1H, chromene-H), 4.80 (s, 2H, -CH_2-O), 4.37 (s, 4H, -CH_2-O (2H), and -CH_2-benzyl (2H)), 2.31 (s, 3H, -CH_3); ^{13}C NMR (100 MHz, $CDCl_3$): δ 171.3, 168.0, 165.2, 162.5, 157.6, 153.2, 138.1, 137.1, 132.4, 129.4, 128.3, 127.9, 125.7, 123.8, 123.0, 116.7, 115.3, 103.9, 90.7 (Ar-C), 67.1, 63.4 (-CH_2-O), 35.2 (-CH_2-benzyl), 21.3 (-CH_3); LCMS (ESI): m/z calcd. for $C_{23}H_{20}N_2O_4S$: 420.4809; found: 421.1351 $[M + H]^+$.

*4-(3-((2-((3-Methylbenzyl)thio)pyrimidin-4-yl)oxy) propoxy)-2H-chromen-2-one (**5f**) (PC-06).* **4b** (100 mg, 0.430 mmol) was coupled with **2b** (103 mg, 0.430 mmol) by means of K_2CO_3 (119 mg, 0.861 mmol) in refluxing acetone. After reaction completion, the crude obtained was purified by column chromatography. Compound **5f** was obtained as a white solid (180 mg, 96% yield). MP: 94−96 °C; ^{1}H NMR (400 MHz, $CDCl_3$): δ 8.24 (d, J = 5.6 Hz, 1H, pyrimidine-H), 7.78 (d, J = 8.0 Hz, 1H, chromene-H), 7.60−7.46 (m, 1H, chromene-H), 7.30 (d, J = 8.0 Hz, 1H, chromene-H), 7.30−7.12 (m, 4H, chromene-H (1H), and -C_6H_4 (3H)), 7.04 (d, J = 6.4 Hz, 1H, -C_6H_4), 6.40 (d, J = 5.6 Hz, 1H, pyrimidine-H), 5.69 (s, 1H, chromene-H), 4.63−4.50 (m, 2H, -CH_2-O), 4.35 (s, 2H, -CH_2-benzyl), 4.32−4.19 (m, 2H, -CH_2-O), 2.41−2.26 (m, 5H, -CH_2-O (2H), and −CH_3 (3H)); ^{13}C NMR (100 MHz, $CDCl_3$): δ 171.4, 168.3, 165.4, 162.7, 157.4, 153.3, 138.1, 137.2, 132.4, 129.6, 128.4, 127.9, 125.9, 123.9, 122.9, 116.8, 115.6, 103.9, 90.7 (Ar-C), 65.8, 62.6 (-CH_2-O), 35.3 (-CH_2-benzyl), 28.1 (-CH_2-), 21.3 (-CH_3); LCMS (ESI): m/z calcd. for $C_{24}H_{22}N_2O_4S$: 434.5075; found: 435.1477 $[M + H]^+$.

*6-Fluoro-4-(2-((2-((3-methylbenzyl)thio)pyrimidin-4-yl)-oxy)ethoxy)-2H-chromen-2-one (**5g**) (PC-07).* **4b** (100 mg, 0.430 mmol) was coupled with **2c** (124 mg, 0.430 mmol) by means of K_2CO_3 (119 mg, 0.861 mmol) in refluxing acetone. After reaction completion, the crude obtained was purified by column chromatography. Compound **5g** was obtained as a white solid (174 mg, 92% yield). MP: 102−104 °C; ^{1}H NMR (400 MHz, $CDCl_3$): δ 8.28 (d, J = 5.6 Hz, 1H, pyrimidine-H), 7.43 (d, J = 6.8 Hz, 1H, chromene-H), 7.31−7.12 (m, 5H, chromene-H (2H), and -C_6H_4 (3H)), 7.06 (d, J = 6 Hz, 1H, -C_6H_4), 6.45 (d, J = 5.2 Hz, 1H, pyrimidine-H), 5.70 (s, 1H, chromene-H), 4.79 (s, 2H, -CH_2-O), 4.37 (s, 4H, -CH_2-O (2H) and -CH_2-benzyl (2H)), 2.32 (s, 3H, -CH_3); ^{13}C NMR (100 MHz, $CDCl_3$): δ 171.4, 168.0, 164.4, 162.1, 159.8, 157.7, 157.4, 149.4, 138.2, 137.1, 129.5, 128.4, 128.0, 125.8, 120.1, 119.9, 118.4, 118.3, 116.4, 116.3, 109.0, 108.8, 103.9, 91.5 (Ar-C), 67.4, 63.4 (-CH_2-O), 35.3 (-CH_2-benzyl), 21.4 (-CH_3); LCMS (ESI): m/z calcd. for $C_{23}H_{19}FN_2O_4S$: 438.4714; found: 439.1230 $[M + H]^+$.

*6-Fluoro-4-(3-((2-((3-methylbenzyl)thio)pyrimidin-4-yl)-oxy)propoxy)-2H-chromen-2-one (**5h**) (PC-08).* **4b** (100 mg, 0.430 mmol) was coupled with **2d** (110 mg, 0.430 mmol) by means of K_2CO_3 (119 mg, 0.861 mmol) in refluxing acetone. After reaction completion, the crude obtained was purified by column chromatography. Compound **5h** was obtained as a white solid (179 mg, 92% yield). MP: 68−70 °C; ^{1}H NMR (400 MHz, $CDCl_3$): δ 8.25 (d, J = 5.2 Hz, 1H, pyrimidine-H), 7.45 (d, J = 7.2 Hz, 1H, chromene-H), 7.31−7.14 (m, 5H, chromene-H (2H), and -C_6H_4 (3H)), 7.05 (s, 1H, -C_6H_4), 6.41 (d, J = 5.2 Hz, 1H, pyrimidine-H), 5.72 (s, 1H, chromene-H), 4.56 (t, J = 5.2 Hz, 2H, -CH_2-O), 4.35 (s, 2H, -CH_2-benzyl), 4.26 (t, J = 5.2 Hz, 2H, -CH_2-O), 2.41−2.27 (m, 5H, -CH_2- (2H), and −CH_3 (3H)); ^{13}C NMR (100 MHz, $CDCl_3$): δ 171.4, 168.3, 164.5, 162.4, 159.8, 157.5, 157.4, 149.4, 138.1, 137.2, 129.6, 128.4, 127.9, 125.9, 120.1, 119.8, 118.5, 118.4, 116.5, 116.4, 108.9, 108.6, 103.9, 91.4 (Ar-C), 66.1, 62.6 (-CH_2-O), 35.3 (-CH_2-benzyl), 28.0 (-CH_2-), 21.4 (−CH_3);LCMS (ESI): m/z calcd. for $C_{24}H_{21}FN_2O_4S$: 452.4979; found: 453.1504 $[M + H]^+$.

*4-(2-((2-((4-Chlorobenzyl)thio)pyrimidin-4-yl)oxy) ethoxy)-2H-chromen-2-one (**5i**) (PC-09).* **4c** (100 mg, 0.396 mmol) was coupled with **2a** (106 mg, 0.396 mmol) by means of K_2CO_3 (109 mg, 0.791 mmol) in refluxing acetone. After reaction completion, the crude obtained was purified by column chromatography. Compound **5i** was obtained as a white solid (153 mg, 88% yield). MP: 128−130 °C; ^{1}H NMR (400 MHz, $CDCl_3$): δ 8.27 (d, J = 5.6 Hz, 1H, pyrimidine-H), 7.75 (dd, J = 8.0, 1.2 Hz, 1H, chromene-H), 7.61−7.47 (m, 1H, chromene-H), 7.36 (d, J = 8.4 Hz, 2H, -C_6H_4), 7.31 (d, J = 8.4 Hz, 1H, chromene-H), 7.32−7.16 (m, 3H, chromene-H (1H), and -C_6H_4 (2H)), 6.46 (d, J = 5.6 Hz, 1H, pyrimidine-H), 5.69 (s, 1H, chromene-H), 4.79 (t, J = 4.4 Hz, 2H, -CH_2-O), 4.41 (t, J = 4.4 Hz, 2H, -CH_2-O), 4.36 (s, 2H, -CH_2-benzyl); ^{13}C NMR (100 MHz, $CDCl_3$): δ 171.0, 168.3, 165.4, 162.7, 157.8, 153.5, 136.3, 133.1, 132.7, 130.3, 128.8, 124.1, 123.2, 116.9, 115.5, 104.4, 91.0 (Ar-C), 67.3, 63.6 (-CH_2-O), 34.7 (-CH_2-benzyl); LCMS (ESI): m/z calcd. for $C_{22}H_{17}ClN_2O_4S$: 440.8994; found: 441.0851 $[M + H]^+$, 443.0818 $[M + 2H]^+$.

Cell Culture Studies on the Vero Cell Line. The Vero cell line (ATCC, CCL-81) was cultured at 37 °C in Dulbecco's modified Eagle's medium (DMEM, Gibco, Grand Island) supplemented with 10% fetal bovine serum (FBS, Gibco) in the atmosphere with 5% CO_2. Cells were digested with 0.25% trypsin and uniformly seeded in 96-well plates with a density of 2×10^4 cells/well prior to infection or drug feeding.

The A549 cell line was procured from ATCC; stock cells were cultured in F-12K media supplemented with 10% inactivated fetal bovine serum (FBS), penicillin (100 IU/mL), and streptomycin (100 μg/mL) in a humidified atmosphere of 5% CO_2 at 37 °C until confluent. The cell was dissociated with a cell dissociating solution (0.2% trypsin, 0.02% EDTA, 0.05% glucose in PBS). The viability of the cells was checked and centrifuged. Further, 50,000 cells/well were seeded in a 96-well plate and incubated for 24 h at 37 °C in a 5% CO_2 incubator.

Antiviral Activity Assay. We evaluated the antiviral efficiency of HTCAs against the SARS-CoV-2 virus *in vitro*. Vero cells were seeded into 96-well plates at a density of 2×10^4 cells/well and then grown for 24 h. The Vero cells were infected at a multiplicity of infection (MOI) of 0.01 (200 PFU/well) for 2 h at 37 °C. Virus input was washed with DMEM, and then, the cells were treated with a medium containing various concentrations (1.5, 3.75, 7.5, 15, 25, and 50 μM) for 48 h. The supernatant was collected, and the RNA was extracted and analyzed by relative quantification by RT-PCR.

The monolayer of A549 cell culture was trypsinized, and the cell count was adjusted to 5×10^4 cells/mL using respective media containing 10% FBS. To each well of the 96-well microtiter plate, 100 μL of the diluted cell suspension (50,000 cells/well) was added. After 24 h, when a partial monolayer was formed, the supernatant was flicked off, the monolayer was washed once with a medium, and 100 μL each of different test

https://doi.org/10.1021/acsomega.3c02079
ACS Omega 2023, 8, 27056−27066

concentrations of test drugs were added onto the partial monolayer in microtiter plates. The plates were then incubated at 37 °C for 24 h in a 5% CO_2 atmosphere. After 24 h incubation, the cells were infected with human coronavirus 229E (HCoV-229E) with 10^4 $TCID_{50}$/100 μL and incubated for 24 h. Post viral infection, the supernatants were removed and 100 μL of MTT (5 mg/10 mL of MTT in PBS) was added to each well. The plates were incubated for 4 h at 37 °C in a 5% CO_2 atmosphere.[54] The supernatant was removed, 100 μL of DMSO was added, and the plates were gently shaken to solubilize the formed formazan. The absorbance was measured using a microplate reader at a wavelength of 590 nm. The percentage inhibition of cytopathic effect (CPE) was calculated using the following formula and the concentration of the test compound needed to inhibit CPE by 50% (IC_{50}) values is generated from the dose−response curves for the cell line. The Oseltamivir drug was taken as a control.

$$\%\ \text{CPE inhibition} = ((\text{OD of control} - \text{OD of sample}) / \text{OD of control}) \times 100$$

RNA Extraction and RT-qPCR Assay. Viral RNA was extracted from 100 μL of supernatant of infected cells using the automated nucleic acid extraction system following the manufacturer's recommendations. SARS-CoV-2 virus detection was performed using the SSIII QRT PCR (Invitrogen, USA) on BioRad Realtime PCR System (BioRad, USA). A standard curve was generated by determination of copy numbers from serial dilutions (10^3−10^9 copies) of the IVT as described earlier.[55]

Molecular Docking Studies. Discovery Studio (DS) version 2.5 software was used in the present study. ChemBioDraw version 8.0 was used to draw the 2-D structure of lead HTCAs. The 3-D structure of RdRp (PDB Id: 74df) protein of SARS-CoV-2 virus was retrieved from PDB database. Suramin cocrystallized protein was considered for molecular docking studies, after removing water molecules, Suramin, and other heteroatoms from the protein. The catalytic site of RdRp was made by using the sphere selection parameter of DS tool. Using the CDOCKER default settings, the molecular docking studies were carried out between the RdRp protein and RTP, Suramin, and lead HTCAs manually one after the other. The Discovery Studio 2.5 platform was used to visualize and study the 2-D, 3-D, and surface view of ligand interaction with the RdRp Protein.

Animals and Husbandry. Wistar Albino rats (weight 150−200 g, 8−10 weeks old) were housed under an ambient condition (temperature of 20−25 °C and relative humidity of 45−55% with a 12/12 h light/dark cycle). Animals were acclimatized for 5 days before the start of the study. They were provided with standard rat chow and mineral water ad libitum. Experimental procedures were performed in accordance with the ethical guidelines for the study and were approved by the Institutional Animal Ethical Committee (JSSAHER/CPT/IAEC/057/2020), JSS Medical College, Mysuru, India.

Acute Oral Toxicity. The study was conducted according to OECD test guideline 423, Acute Toxic Class Method (Adopted on December 17, 2001) with minor modifications. Female animals were administered with a single dose of compound **5d** at 300 and 2000 mg/kg, p.o. and observed for mortality, morbidity, body weight change, feed intake, and clinical signs of toxicity for 14 days.

Oral Bioavailability. Animals received a single prefixed dose (10 mg/kg, p.o) of compound **5d** after being overnight fasted, but with free access to water. Blood samples were collected at 0 min, 5 min, 1 h, 6 h, 24 h, 36 h, and 48 h (3 animals/time point) through a retro-orbital puncture under mild anesthesia, and plasma was separated and stored at −20 °C.

Chromatography Conditions. Analytical separation was performed using a Phenomenox luna C8 Column (250 mm × 4.5 μm, 5 μm) equipped with an Auto sampler. 0.1% formic acid in methanol was used as the mobile phase (Shimadzu LC2030). The other chromatographic conditions used were as follows: flow rate, 1.5 mL/min; oven temperature: 25 ± 5 °C; injection volume, 10 μL.

Preparation of Standard Solutions for Linearity. 5 mg of the sample was diluted in 5 mL of methanol (HPLC grade) to make the concentration 1000 μg/mL. Later, 0.5, 1, 1.5, 2.0, 2.5, and 3.0 mL of the stock solution were pipetted out and diluted to 10 mL of methanol to obtain the concentrations of 50, 100, 150, 200, 250, and 300 μg/mL, and from the solutions, linearity ranges of 5, 10, 15, 20, 25, and 30 μg/mL were prepared by mixing 200 μL of each concentration with 100 μL of the blank plasma, vortexed for 20 s, made up to 2 mL using methanol, and centrifuged at 10,000 RPM for 10 min at 4 °C. The supernatant was filtered through syringe filters of pore size 0.22 μm and used for chromatographic analysis.

Mouse, Rat, and Human Liver-Microsome Stability Assay. This experiment was carried out with mouse, rat, and liver microsomes to evaluate the metabolic stability of title compounds. The compounds **5f**, **5h**, **5d**, and **5e** were of interest and were tested at 1 μM by incubating with microsomes + NADPH for 30 min at 37 °C. The reaction was stopped by adding acetonitrile containing an internal standard. Samples were extracted and centrifuged to obtain supernatant fractions. Supernatants were submitted for LCMS/MS analysis. Simultaneously, a "0" minute control was included, in which the reaction was immediately stopped with acetonitrile and processed as detailed. Reference control compounds of known metabolism (Verapamil, high metabolism; Atenolol, low metabolism) were also included. Another control, namely, "minus NADPH" (all reagents except for microsome), was included and processed in similar conditions, and the stability of the test compound was evaluated in a buffer during incubation.

Use of the vNN Web Server. Around 15 ADMET parameters were determined using the vNN Web Server by querying each molecule into the web portal after logging in to the server (https://vnnadmet.bhsai.org/). The obtained results were tabulated and analyzed.

Statistical Analysis. Data were expressed as mean±SD. Plasma concentration values below the lower limit of quantitation (LLOQ) of the assay (1 μg/mL) were assigned a value of zero (μg/mL) for the purpose of mean calculation. If the resulting mean concentration returned a value below the LLOQ, it was treated as below level of quantification. The area under the test article serum concentration vs. time curve (AUC) was calculated using the linear trapezoidal method (linear interpolation). PK parameters describing the systemic exposure of the test article in the test system were estimated from observed (rather than predicted) plasma concentration values and the maximum value (Cmax), the dosing regimen, the AUC, and the terminal elimination phase rate constant (Kel) for each group. The PK profiles were characterized by noncompartmental analysis of **5d** serum concentration data

https://doi.org/10.1021/acsomega.3c02079
ACS Omega 2023, 8, 27056−27066

with targeted sampling time points using validated computer software (WinNonlin, version 3.2, California).

■ ASSOCIATED CONTENT

Supporting Information

The Supporting Information is available free of charge at https://pubs.acs.org/doi/10.1021/acsomega.3c02079.

Compounds' characterization, antiviral activity graph, and phamacokinetics data (PDF)

■ AUTHOR INFORMATION

Corresponding Authors

Basappa Basappa − *Laboratory of Chemical Biology, Department of Studies in Organic Chemistry, University of Mysore, Mysore 570006, India*; orcid.org/0000-0002-8844-468X; Email: salundibasappa@gmail.com

Pragya D. Yadav − *Indian Council of Medical Research-National Institute of Virology (ICMR-NIV), Pune, Maharashtra 411021, India*; Email: hellopragya22@gmail.com

Authors

Divakar Vishwanath − *Laboratory of Chemical Biology, Department of Studies in Organic Chemistry, University of Mysore, Mysore 570006, India*

Anita Shete-Aich − *Indian Council of Medical Research-National Institute of Virology (ICMR-NIV), Pune, Maharashtra 411021, India*

Manjunath B. Honnegowda − *DRM innovations PVT.LTD, Mysore 570029, India*

Mahesh Padukudru Anand − *Department of Respiratory Medicine, JSS Medical College, and Hospital, JSS Academy of Higher Education & Research, Mysore 570015 Karnataka, India*

Saravana Babu Chidambaram − *Department of Pharmacology, JSS College of Pharmacy, JSS Academy of Higher Education & Research, Mysore 570015 Karnataka, India*

Gajanan Sapkal − *Indian Council of Medical Research-National Institute of Virology (ICMR-NIV), Pune, Maharashtra 411021, India*

Complete contact information is available at: https://pubs.acs.org/10.1021/acsomega.3c02079

Author Contributions

D.V. and A.S.A. performed the experiments. M.H., M.P.A., S.C., and G.S. provided resources and were involved in the study design. P.D.Y and B.B. designed the work, provided resources, and wrote the manuscript.

Funding

The chemistry laboratory was supported by funding from the Council of Scientific and Industrial Research (No. 02(0291)17/EMR-II), the Department of Biotechnology-NER, and the Vision Group on Science and Technology, Government of Karnataka. The antiviral testing at ICMR-NIV, Pune, is supported through intramural funding from the Indian Council of Medical Research, New Delhi, under the COVID-19 fund. D.V. thanks DST PhD Fellowship from KSTePS, Karnataka, for providing stipend.

Notes

The authors declare no competing financial interest.

■ ACKNOWLEDGMENTS

The authors acknowledge the technical support of Mr. Prasad Sarkale, Mr. Srikant Baradkar, Mr. Rajen Lakra, and Dr. Sharda Sharma of ICMR-NIV, Pune.

■ ABBREVIATIONS

CCR2, CC chemokine receptor 2; CCL2, CC chemokine ligand 2; CCR5, CC chemokine receptor 5; TLC, thin-layer chromatography

■ REFERENCES

(1) Liu, C.; Zhou, Q.; Li, Y.; Garner, L. V.; Watkins, S. P.; Carter, L. J.; Smoot, J.; Gregg, A. C.; Daniels, A. D.; Jervey, S.; Albaiu, D. Research and Development on Therapeutic Agents and Vaccines for COVID-19 and Related Human Coronavirus Diseases. *ACS Cent. Sci.* **2020**, *6*, 315−331.

(2) Hao, W.; Li, M.; Huang, X. First Atypical Case of 2019 Novel Coronavirus in Yan'an, China. *Clin. Microbiol. Infect.* **2020**, *26*, 952−953.

(3) Hui, D. S.; I Azhar, E.; Madani, T. A.; Ntoumi, F.; Kock, R.; Dar, O.; Ippolito, G.; Mchugh, T. D.; Memish, Z. A.; Drosten, C.; Zumla, A.; Petersen, E. The Continuing 2019-NCoV Epidemic Threat of Novel Coronaviruses to Global Health — the Latest 2019 Novel Coronavirus Outbreak in Wuhan, China. *Int. J. Infect. Dis.* **2020**, *91*, 264−266.

(4) Khan, S.; Kale, M.; Siddiqui, F.; Nema, N. Novel Pyrimidine-Benzimidazole Hybrids with Antibacterial and Antifungal Properties and Potential Inhibition of SARS-CoV-2 Main Protease and Spike Glycoprotein. *Digital Chin. Med.* **2021**, *4*, 102−119.

(5) Scudellari, M. How the Coronavirus Infects Cells — and Why Delta Is so Dangerous. *Nature* **2021**, *595*, 640−644.

(6) Singh, J.; Rahman, S. A.; Ehtesham, N. Z.; Hira, S.; Hasnain, S. E. SARS-CoV-2 Variants of Concern Are Emerging in India. *Nat. Med.* **2021**, *27*, 1131−1133.

(7) World Health Organization. *WHO Coronavirus Disease (COVID-19) Dashboard*. Who.int. https://covid19.who.int.

(8) Abu-Zaied, M. A.; Elgemeie, G. H.; Mahmoud, N. M. Anti-Covid-19 Drug Analogues: Synthesis of Novel Pyrimidine Thioglycosides as Antiviral Agents against SARS-COV-2 and Avian Influenza H5N1 Viruses. *ACS Omega* **2021**, *6*, 16890−16904.

(9) Rabie, A. M. Potent Inhibitory Activities of the Adenosine Analogue Cordycepin on SARS-CoV-2 Replication. *ACS Omega* **2022**, *7*, 2960−2969.

(10) Rabie, A. M. Potent Toxic Effects of Taroxaz-104 on the Replication of SARS-CoV-2 Particles. *Chem.-Biol. Interact.* **2021**, *343*, No. 109480.

(11) Puranik, A.; Lenehan, P. J.; Silvert, E.; Niesen, M. J. M.; Corchado-Garcia, J.; O'Horo, J. C.; Virk, A.; Swift, M. D.; Halamka, J.; Badley, A. D.; Venkatakrishnan, A. J.; Soundararajan, V. Comparison of Two Highly-Effective MRNA Vaccines for COVID-19 during Periods of Alpha and Delta Variant Prevalence *medRxiv [Preprint]* 2021, DOI: 10.2139/ssrn.3902782.

(12) Lopez Bernal, J.; Andrews, N.; Gower, C.; Gallagher, E.; Simmons, R.; Thelwall, S.; Stowe, J.; Tessier, E.; Groves, N.; Dabrera, G.; Myers, R.; Campbell, C. N. J.; Amirthalingam, G.; Edmunds, M.; Zambon, M.; Brown, K. E.; Hopkins, S.; Chand, M.; Ramsay, M. Effectiveness of Covid-19 Vaccines against the B.1.617.2 (Delta) Variant. *N. Engl. J. Med.* **2021**, *385*, 585−594.

(13) Gupta, R. K. Author Correction: Will SARS-CoV-2 variants of concern affect the promise of vaccines. *Nat. Rev. Immunol.* **2021**, *21*, 405−405.

(14) Awadasseid, A.; Wu, Y.; Tanaka, Y.; Zhang, W. Effective Drugs Used to Combat SARS-CoV-2 Infection and the Current Status of Vaccines. *Biomed. Pharmacother.* **2021**, *137*, No. 111330.

(15) Brindani, N.; Munafò, F.; Menichetti, A.; Donati, E.; Nigro, M.; Ottonello, G.; Armirotti, A.; De Vivo, M. Design, Synthesis, Docking,

and Biochemical Characterization of Non-Nucleoside SARS-CoV-2 RdRp Inhibitors. *Bioorg. Med. Chem.* **2023**, *80*, No. 117179.
(16) Uengwetwanit, T.; Chutiwitoonchai, N.; Wichapong, K.; Karoonuthaisiri, N. Identification of Novel SARS-CoV-2 RNA Dependent RNA Polymerase (RdRp) Inhibitors: From in Silico Screening to Experimentally Validated Inhibitory Activity. *Comput. Struct. Biotechnol. J.* **2022**, *20*, 882−890.
(17) Vicenti, I.; Zazzi, M.; Saladini, F. SARS-CoV-2 RNA-Dependent RNA Polymerase as a Therapeutic Target for COVID-19. *Expert Opin. Ther. Pat.* **2021**, *31*, 325−337.
(18) Eltahla, A. A.; Luciani, F.; White, P. A.; Lloyd, A. R.; Bull, R. A. Inhibitors of the Hepatitis c Virus Polymerase; Mode of Action and Resistance. *Viruses* **2015**, *7*, 5206−5224.
(19) Madhvi, A.; Hingane, S.; Srivastav, R.; Joshi, N.; Subramani, C.; Muthumohan, R.; Khasa, R.; Varshney, S.; Kalia, M.; Vrati, S.; Surjit, M.; Ranjith-Kumar, C. T. A Screen for Novel Hepatitis c Virus RdRp Inhibitor Identifies a Broad-Spectrum Antiviral Compound. *Sci. Rep.* **2017**, *7*, No. 5816.
(20) Nascimento, I. J. d. S.; Santos-Júnior, P. F. d. S.; Aquino, T. M.; Araújo-Júnior, J. X. d.; Silva-Júnior, E. F. d. Insights on Dengue and Zika NS5 RNA-Dependent RNA Polymerase (RdRp) Inhibitors. *Eur. J. Med. Chem.* **2021**, *224*, No. 113698.
(21) Shimizu, H.; Saito, A.; Mikuni, J.; Nakayama, E. E.; Koyama, H.; Honma, T.; Shirouzu, M.; Sekine, S.; Shioda, T. Discovery of a Small Molecule Inhibitor Targeting Dengue Virus NS5 RNA-Dependent RNA Polymerase. *PLoS Neglected Trop. Dis.* **2019**, *13*, No. e0007894.
(22) Chen, Y.; Chi, X.; Zhang, H.; Zhang, Y.; Qiao, L.; Ding, J.; Han, Y.; Lin, Y.; Jiang, J. Identification of Potent Zika Virus NS5 RNA-Dependent RNA Polymerase Inhibitors Combining Virtual Screening and Biological Assays. *Int. J. Mol. Sci.* **2023**, *24*, 1900.
(23) Massari, S.; Desantis, J.; Nizi, M. G.; Cecchetti, V.; Tabarrini, O. Inhibition of Influenza Virus Polymerase by Interfering with Its Protein−Protein Interactions. *ACS Infect. Dis.* **2021**, *7*, 1332−1350.
(24) Peng, S.; Wang, H.; Wang, Z.; Wang, Q. Progression of Antiviral Agents Targeting Viral Polymerases. *Molecules* **2022**, *27*, 7370.
(25) Goswami, D. Comparative Assessment of RNA-Dependent RNA Polymerase (RdRp) Inhibitors under Clinical Trials to Control SARS-CoV2 Using Rigorous Computational Workflow. *RSC Adv.* **2021**, *11*, 29015−29028.
(26) Kim, J. H.; Marks, F.; Clemens, J. D. Looking beyond COVID-19 Vaccine Phase 3 Trials. *Nat. Med.* **2021**, *27*, 205−211.
(27) Pillaiyar, T.; Flury, P.; Krüger, N.; Su, H.; Schäkel, L.; Barbosa Da Silva, E.; Eppler, O.; Kronenberger, T.; Nie, T.; Luedtke, S.; Rocha, C.; Sylvester, K.; Petry, M. R. I.; McKerrow, J. H.; Poso, A.; Pöhlmann, S.; Gütschow, M.; O'Donoghue, A. J.; Xu, Y.; Müller, C. E.; Laufer, S. A. Small-Molecule Thioesters as SARS-CoV-2 Main Protease Inhibitors: Enzyme Inhibition, Structure−Activity Relationships, Antiviral Activity, and X-Ray Structure Determination. *J. Med. Chem.* **2022**, *65*, 9376−9395.
(28) Jayk Bernal, A.; Gomes da Silva, M. M.; Musungaie, D. B.; Kovalchuk, E.; Gonzalez, A.; Delos Reyes, V.; Martín-Quirós, A.; Caraco, Y.; Williams-Diaz, A.; Brown, M. L.; Du, J.; Pedley, A.; Assaid, C.; Strizki, J.; Grobler, J. A.; Shamsuddin, H. H.; Tipping, R.; Wan, H.; Paschke, A.; Butterton, J. R.; et al.*et al.* Molnupiravir for Oral Treatment of Covid-19 in Nonhospitalized Patients. *N. Engl. J. Med.* **2022**, *386*, 509−520.
(29) Eltayb, W. A.; Abdalla, M.; Rabie, A. M. Novel Investigational Anti-SARS-CoV-2 Agent Ensitrelvir "S-217622": A Very Promising Potential Universal Broad-Spectrum Antiviral at the Therapeutic Frontline of Coronavirus Species. *ACS Omega* **2023**, *8*, 5234−5246.
(30) Rabie, A. M.; Eltayb, W. A. Potent Dual Polymerase/Exonuclease Inhibitory Activities of Antioxidant Aminothiadiazoles against the COVID-19 Omicron Virus: A Promising in Silico/in Vitro Repositioning Research Study. *Molecular Biotechnology* **2023**, 1−20.
(31) Yin, W.; Mao, C.; Luan, X.; Shen, D.-D.; Shen, Q.; Su, H.; Wang, X.; Zhou, F.; Zhao, W.; Gao, M.; Chang, S.; Xie, Y.-C.; Tian, G.; Jiang, H.-W.; Tao, S.-C.; Shen, J.; Jiang, Y.; Jiang, H.; Xu, Y.; Zhang, S.; Zhang, Y.; Xu, H. E. Structural Basis for Inhibition of the RNA-Dependent RNA Polymerase from SARS-CoV-2 by Remdesivir. *Science* **2020**, *368*, 1499−1504.
(32) Chien, M.; Anderson, T. K.; Jockusch, S.; Tao, C.; Li, X.; Kumar, S.; Russo, J. J.; Kirchdoerfer, R. N.; Ju, J. Nucleotide Analogues as Inhibitors of SARS-CoV-2 Polymerase, a Key Drug Target for COVID-19. *J. Proteome Res.* **2020**, *19*, 4690−4697.
(33) Zhang, J.-L.; Li, Y.-H.; Wang, L.-L.; Liu, H.-Q.; Lu, S.-Y.; Liu, Y.; Li, K.; Liu, B.; Li, S.-Y.; Shao, F.-M.; Wang, K.; Sheng, N.; Li, R.; Cui, J.-J.; Sun, P.-C.; Ma, C.-X.; Zhu, B.; Wang, Z.; Wan, Y.-H.; Yu, S.-S.; et al.*et al.* Azvudine Is a Thymus-Homing Anti-SARS-CoV-2 Drug Effective in Treating COVID-19 Patients. *Signal Transduction Targeted Ther.* **2021**, *6*, 414.
(34) Rabie, A. M.; Eltayb, W. A. Strong Dual Antipolymerase/Antiexonuclease Actions of Some Aminothiadiazole Antioxidants: A Promising In-Silico/In-Vitro Repurposing Research Study against the COVID-19 Omicron Virus (B.1.1.529.3 Lineage). *Adv. Redox Res.* **2023**, No. 100064.
(35) Dejmek, M.; Konkoľová, E.; Eyer, L.; Straková, P.; Svoboda, P.; Šála, M.; Krejčová, K.; Růžek, D.; Boura, E.; Nencka, R. Non-Nucleotide RNA-Dependent RNA Polymerase Inhibitor That Blocks SARS-CoV-2 Replication. *Viruses* **2021**, *13*, 1585.
(36) Yin, W.; Luan, X.; Li, Z.; Zhou, Z.; Wang, Q.; Gao, M.; Wang, X.; Zhou, F.; Shi, J.; You, E.; Liu, M.; Wang, Q.; Jiang, Y.; Jiang, H.; Xiao, G.; Zhang, L.; Yu, X.; Zhang, S.; Eric Xu, H. Structural Basis for Inhibition of the SARS-CoV-2 RNA Polymerase by Suramin. *Nat. Struct. Mol. Biol.* **2021**, *28*, 319−325.
(37) Jin, Y.-H.; Min, J. S.; Jeon, S.; Lee, J.; Kim, S.; Park, T.; Park, D.; Jang, M. S.; Park, C. M.; Song, J. H.; Kim, H. R.; Kwon, S. Lycorine, a Non-Nucleoside RNA Dependent RNA Polymerase Inhibitor, as Potential Treatment for Emerging Coronavirus Infections. *Phytomedicine* **2021**, *86*, No. 153440.
(38) Zhang, G.-N.; Zhao, J.; Li, Q.; Wang, M.; Zhu, M.; Wang, J.; Cen, S.; Wang, Y. Discovery and Optimization of 2-((1H-Indol-3-Yl)Thio)-N-Benzyl-Acetamides as Novel SARS-CoV-2 RdRp Inhibitors. *Eur. J. Med. Chem.* **2021**, *223*, No. 113622.
(39) Zhao, J.; Zhang, Y.; Wang, M.; Liu, Q.; Lei, X.; Wu, M.; Guo, S.; Yi, D.; Li, Q.; Ma, L.; Liu, Z.; Guo, F.; Wang, J.; Li, X.; Wang, Y.; Cen, S. Quinoline and Quinazoline Derivatives Inhibit Viral RNA Synthesis by SARS-CoV-2 RdRp. *ACS Infect. Dis.* **2021**, *7*, 1535−1544.
(40) Alamshany, Z. M.; Khattab, R. R.; Hassan, N. A.; El-Sayed, A. A.; Tantawy, M. A.; Mostafa, A.; Hassan, A. A. Synthesis and Molecular Docking Study of Novel Pyrimidine Derivatives against COVID-19. *Molecules* **2023**, *28*, 739.
(41) Cherian, S. S.; Agrawal, M.; Basu, A.; Abraham, P.; Gangakhedkar, R. R.; Bhargava, B. Perspectives for Repurposing Drugs for the Coronavirus Disease 2019. *Indian J. Med. Res.* **2020**, *151*, 160−171.
(42) Lee, J.-H.; Alam, I.; Han, K. R.; Cho, S.; Shin, S.; Kang, S.; Yang, J. M.; Kim, K. H. Crystal Structures of Murine Norovirus-1 RNA-Dependent RNA Polymerase. *J. Gen. Virol.* **2011**, *92*, 1607−1616.
(43) Chandramohanadas, R.; Basappa; Russell, B.; Liew, K.; Yau, Y. H.; Chong, A.; Liu, M.; Gunalan, K.; Raman, R.; Renia, L.; Nosten, F.; Shochat, S. G.; Dao, M.; Sasisekharan, R.; Suresh, S.; Preiser, P. Small Molecule Targeting Malaria Merozoite Surface Protein-1 (MSP-1) Prevents Host Invasion of Divergent Plasmodial Species. *J. Infect. Dis.* **2014**, *210*, 1616−1626.
(44) Anusha, S.; Cp, B.; Mohan, C. D.; Mathai, J.; Rangappa, S.; Mohan, S.; Chandra; Paricharak, S.; Mervin, L.; Fuchs, J. E.; M, M.; Bender, A.; Basappa; Rangappa, K. S. A Nano-MgO and Ionic Liquid-Catalyzed "Green" Synthesis Protocol for the Development of Adamantyl-Imidazolo-Thiadiazoles as Anti-Tuberculosis Agents Targeting Sterol 14α-Demethylase (CYP51). *PLoS One* **2015**, *10*, No. e0139798.
(45) Ramaswamy, R. S.; Prathyusha, N.; Saranya, R.; Sumathy, H.; Mohanavalli, K. T.; Priya, R. J.; Venkhatesh, J. R.; Babu, C. S.; Manickavasakam, K.; Thanikachalam, S. Acute Toxicity and the 28-

https://doi.org/10.1021/acsomega.3c02079
ACS Omega 2023, 8, 27056−27066

Day Repeated Dose Study of a Siddha Medicine Nuna Kadugu in Rats. *BMC Complementary Altern. Med.* **2012**, *12*, 190.
(46) Choezom, L.; Chandan, R. S.; Gurupadayya, B. M.; Barath, M. Method Development and Validation of Glucosamine in Marketed Tablet Using RP-HPLC Method. *Int. J. Pharm. Res. Scholars* **2021**, *13*, 1850.
(47) Baranczewski, P.; Stańczak, A.; Sundberg, K.; Svensson, R.; Wallin, A.; Jansson, J.; Garberg, P.; Postlind, H. Introduction to in Vitro Estimation of Metabolic Stability and Drug Interactions of New Chemical Entities in Drug Discovery and Development. *Pharmacol. Rep.* **2006**, *58*, 453−472.
(48) Basappa, B.; Chumadathil Pookunoth, B.; Shinduvalli Kempasiddegowda, M.; Knchugarakoppal Subbegowda, R.; Lobie, P. E.; Pandey, V. Novel Biphenyl Amines Inhibit Oestrogen Receptor (ER)-α in ER-Positive Mammary Carcinoma Cells. *Molecules* **2021**, *26*, 783.
(49) Schyman, P.; Liu, R.; Desai, V.; Wallqvist, A. VNN Web Server for ADMET Predictions. *Front. Pharmacol.* **2017**, *8*, 889.
(50) Kavitha, C. V.; Basappa, null; Swamy, S. N.; Mantelingu, K.; Doreswamy, S.; Sridhar, M. A.; Shashidhara Prasad, J.; Rangappa, K. S. Synthesis of New Bioactive Venlafaxine Analogs: Novel Thiazolidin-4-Ones as Antimicrobials. *Bioorg. Med. Chem.* **2006**, *14*, 2290−2299.
(51) Priya, B. S.; Anil Kumar, C.; Nanjunda Swamy, S.; Basappa, null; Naveen, S.; Shashidhara Prasad, J.; Rangappa, K. S. 2-(2-(2-Ethoxybenzoylamino)-4-Chlorophenoxy)-N-(2-Ethoxybenzoyl)-Benzamine Inhibits EAT Cell Induced Angiogenesis by down Regulation of VEGF Secretion. *Bioorg. Med. Chem. Lett.* **2007**, *17*, 2775−2780.
(52) Basappa; Ananda, C. S.; Swamy, N.; Sugahara, K.; Rangappa, K. S. Anti-Tumor and Anti-Angiogenic Activity of Novel Hydantoin Derivatives: Inhibition of VEGF Secretion in Liver Metastatic Osteosarcoma Cells. *Bioorg. Med. Chem.* **2009**, *17*, 4928−4934.
(53) Swamy, S. N.; Basappa; Priya, B. S.; Prabhuswamy, B.; Doreswamy, B. H.; Prasad, J. S.; Rangappa, K. S. Synthesis of Pharmaceutically Important Condensed Heterocyclic 4,6-Disubstituted-1,2,4-Triazolo-1,3,4-Thiadiazole Derivatives as Antimicrobials. *Eur. J. Med. Chem.* **2006**, *41*, 531−538.
(54) Min, J. S.; Kim, D. E.; Jin, Y.-H.; Kwon, S. Kurarinone Inhibits HCoV-OC43 Infection by Impairing the Virus-Induced Autophagic Flux in MRC-5 Human Lung Cells. *J. Clin. Med.* **2020**, *9*, 2230.
(55) Choudhary, M. L.; Vipat, V.; Jadhav, S.; Basu, A.; Cherian, S.; Abraham, P.; Potdar, V. A. Development of in vitro transcribed RNA as positive control for laboratory diagnosis of SARS-CoV2 in India. *Indian J. Med. Res.* **2020**, *11* (2&3), 251−254.

https://doi.org/10.1021/acsomega.3c02079
ACS Omega 2023, 8, 27056−27066